Tissue Engineering

DOI: 10.1089/ten.TEB.2021.0139

Raman spectroscopy in skeletal tissue disorders and tissue engineering: present and prospective.

Running title: Raman spectroscopy in regenerative orthopaedics

Marco Fosca[1], Valentina Basoli[2], Elena Della Bella[2], Fabrizio Russo[3], Gianluca Vadalà[3], Mauro Alini[2], Julietta V. Rau[1,4*#], Sophie Verrier[2*]

[1]*Istituto di Struttura della Materia, Consiglio Nazionale delle Ricerche (ISM-CNR), Via del Fosso del Cavaliere, 100 - 00133 Rome, Italy*

[2]*AO Research Institute, Clavadelerstrasse 8, 7270 Davos, Switzerland*

[3]*Campus Bio-Medico University, Via Alvaro del Portillo 200, Rome, Italy*

[4]*Sechenov First Moscow State Medical University, Trubetskaya 8, build. 2, 119991 Moscow, Russian Federation*

*Authors with equal contribution. #Corresponding author.

Authors contact information:

Marco Fosca, Istituto di Struttura della Materia, Consiglio Nazionale delle Ricerche (ISM-CNR), Via del Fosso del Cavaliere, 100 - 00133 Rome, Italy, Tel: +39 4993 4509, marco.fosca@ism.cnr.it, http://orcid.org/0000-0003-0962-8083

Valentina Basoli, AO Research Institute, Clavadelerstrasse 8, 7270 Davos, Switzerland, Tel.: +41 81 414 21 11 valentina.basoli@aofoundation.org http://orcid.org/0000-0002-4703-7308

Elena Della Bella, AO Research Institute, Clavadelerstrasse 8, 7270 Davos, Switzerland. Tel.: +41 81 414 21 11 elena.dellabella@aofoundation.org, http://orcid.org/0000-0001-5151-7390

Fabrizio Russo, Campus Bio-Medico University, Via Alvaro del Portillo 200, Rome, Italy, Tel +39 349 3601908 fabrizio.russo@unicampus.it,

Gianluca Vadala, Campus Bio-Medico University, Via Alvaro del Portillo 200, Rome, Italy Tel: +39 338 9831497 G.Vadala@unicampus.it

Mauro Alini, AO Research Institute, Clavadelerstrasse 8, 7270 Davos, Switzerland, Tel.: +41 81 414 21 11 mauro.alini@aofoundation.org, https://orcid.org/0000-0002-0262-1412

Julietta V. Rau, Istituto di Struttura della Materia, Consiglio Nazionale delle Ricerche (ISM-CNR), Via del Fosso del Cavaliere, 100 - 00133 Rome, Italy, and Sechenov First Moscow State Medical University, Trubetskaya 8, build. 2, 119991 Moscow, Russian Federation, Tel + 39 4993 4086 giulietta.rau@ism.cnr.it, http://orcid.org/0000-0002-7953-1853

Sophie Verrier, AO Research Institute, Clavadelerstrasse 8, Davos, Switzerland, Tel.: +41 81 414 21 11 sophie.verrier@aofoundation.org, https://orcid.org/0000-0003-2478-2804

ABSTRACT

Musculoskeletal disorders are the most common reason of chronic pain and disability representing worldwide an enormous socio-economic burden. In this review, new biomedical application fields for Raman spectroscopy (RS) technique related to skeletal tissues are discussed showing that it can provide a comprehensive profile of tissue composition *in situ*, in a rapid, label-free, and non-destructive manner. RS can be used as a tool to study tissue alterations associated to aging, pathologies, and disease treatments. The main advantage with respect to currently applied methods in clinics is its ability to provide specific information on molecular composition, which goes beyond other diagnostic tools. Being compatible with water, RS can be performed without pre-treatment on unfixed, hydrated tissue samples, without any labelling and chemical fixation used in histochemical methods. This review provides first the description of basic principles of RS as a biotechnology tool and introduces into the field of currently available RS based techniques, developed to enhance Raman signal. The main spectral processing statistical tools, fingerprint identification and available databases are mentioned. The recent literature has been analysed for such applications of RS as tendon and ligaments, cartilage, bone, and tissue engineered constructs for regenerative medicine. Several cases of proof-of-concept preclinical studies have been described. Finally, advantages, limitations, future perspectives, and challenges for translation of RS into clinical practice have been also discussed.

IMPACT STATEMENT

Raman Spectroscopy (RS) is a powerful non-invasive tool giving access to molecular vibrations and characteristics of samples in a wavelength window of 600 to 3200 cm^{-1}, thus giving access to a molecular fingerprint of biological samples in a non-destructive way. RS could not only be used in clinical diagnostics, but also for quality control of tissues and tissue-engineered constructs, reducing number of samples, time and the variety of analysis required in the quality control chain before implantation.

INTRODUCTION

Musculoskeletal disorders are the most common cause of severe chronic pain and reduced quality of life representing an enormous socio-economic concern. Approximately 1.71 billion people globally are affected by functioning limitations and disability.[1] Musculoskeletal conditions can either arise suddenly, such as fractures, sprains and strains, or develop from chronic conditions. They affect different tissues of the locomotor system such as bone, cartilage, tendons, and muscles. Each of these tissues presents a highly hierarchical organization ranging from macroscale (fibrils, osteons, etc.) to microscale (proteins) and to nanoscale (molecular composition) structures.

In case of disease or injury, current tissue diagnostics and monitoring techniques are mainly based on macroscopic evaluation methods, such as X-ray, ultrasound, computed tomography, Dual-energy X-ray absorptiometry (DXA), and Magnetic Resonance Imaging (MRI). If necessary, those techniques are combined with histopathological evaluations and marker identification, or/and metabolic activity assays (e.g., bone turnover related proteins in body fluids). If those methods are critical for diagnostics, they provide limited information regarding the molecular status of tissues and their lesions that are often asymptomatic at early stages.

Therefore, other techniques able to increase the reliability of diagnosis and to help through the clinical decision-making process are required. Raman spectroscopy (RS) is very suitable for this goal since it can provide a comprehensive profile of the tissue composition *in situ*, in a rapid, label-free, and non-destructive manner.[2] Indeed, this technique produces a molecular fingerprint of the constituents of a tissue, based on inelastic light scattering.[3] Being compatible with water, RS can be performed on unfixed, hydrated tissue samples, without any manipulations, such as molecular labelling or chemical treatments, which represent potential source of artifacts.

RS is thus a promising *in vivo* tool for various biomedical applications including the musculoskeletal system. In clinical settings, RS was already used to discern aging of tissue and tendon molecular differences,[4] to evaluate the extracellular matrix (ECM) in osteoporotic and osteonecrotic bone[5,6] and to predict fragility fractures.[7] Moreover, it has been used to characterize articular cartilage degeneration[8] and select the optimal treatment strategy during cartilage repair surgery.[9]

The present review is focused on RS principles highlighting its orthopaedic applications. Both basic science and translational studies on musculoskeletal tissues are reviewed. Finally, usefulness, limitations, future perspectives, and challenges for translation of RS into clinical use are also discussed.

RAMAN SPECTROSCOPY

Principle and techniques

RS is an inelastic scattered photon procedure in which one photon is absorbed while another one is emitted. Light getting in contact with transparent fluids emits two types of light scattering: one is determined by the normal optical properties of the atoms or molecules, the other by their fluctuation from normal state.

When light waves interact with a molecule, they modify their vibrational status inducing small changes (shifts) in the scattered light frequency. When the incident light energy is scattered with equal energy, this refers to Rayleigh or elastic scattering. In the case of Raman scattering, the interaction of light with a molecule induces changes in its intrinsic vibrational state (molecular electrons oscillate in response to the light photon excitation). Those changes translate as small shift in the frequency of the scattered light: either through a loss (Stokes, most common case) or a gain of the scattered light energy (anti-Stokes). This is referred to as Raman shift or scattering (inelastic scattering).[10] Raman scattering is thus highly specific to molecular bonds and can be used to both identify molecules and their response to their environment.

A conventional RS set up comprises a laser source - typically in the near infrared as it reduces autofluorescence interferences typical for biological specimens,[11] a series of mirrors, and a microscope directing the light toward the sample. After interaction with the sample, only a small portion of the scattered photons have changed their frequency. Following the filtration of elastically scattered photons, photons with modified frequency are directed toward a spectrometer linked to a detector system (CCD) from which the data are transferred to a computer.

However, Raman signal being very weak, many efforts were placed in finding ways to increase it.[12] As of today, more than 20 RS techniques have been developed and some of them will be described throughout the present review (**Fig.1**).

In spontaneous RS, the Stokes signal is detected under constant radiation. For the RS application *in vivo* for clinical purposes, the light should be delivered directly to the tissue and collected by specifically designed fibre probes;[13,14] however one of the biggest challenges related to the collection of signal with the use of fibre probes is related to tissue autofluorescence.

The above-mentioned issue can be overcome using of confocal RS. The combination of a confocal microscope with a Raman spectroscope improves optical depth acquisition. In confocal RS a spatial filtering of the collected RS light with a pinhole or an optical fibre is applied to block out-of-focus signal. To date, confocal Raman probes are mainly used for *ex vivo* and *in vitro* studies.[15,16]

Compared to RS, spatially offset RS (SORS) collects Raman signal from deeper regions of tissue by spatially offsetting the detection and excitation fibres. Collecting the Raman signal at different offsets effectively samples different layers in the tissue. SORS typically uses a probe with an illumination fibre surrounded by detections fibres offset of 1–5 mm,[17,18] but an offset as high as 16 mm has been used to perform Raman tomographic imaging in bone.[19] Spectra collected by SORS technique are usually characterized by convolution of signals originated at different depths of the investigated specimen and can be considered an unwanted consequence of a relative low depth resolution. Reduced depth resolution relies on two main causes: 1) a relatively limited depth of field in a two-dimensional detector and 2) the geometric aberration induced by axicon lens. These technical limitations can lead to a simple qualitative sampling with a significant cross-talk among different layers.[20]

In the Coherent RS technique, the difference due a vibrational mode frequency generated by two light sources (referred as pump and Stokes beam) results in the acquisition of signal for a specific molecular bond of interest. The coherent addition of the Raman signal from different molecules improves the signal compared to spontaneous Raman, typically by up to ~10^5.[21] Coherent RS techniques include stimulated Raman spectroscopy (SRS) and coherent anti-Stokes Raman spectroscopy (CARS). Both SRS and CARS can be performed in highly fluorescent media, which is usually a limiting factor for Raman imaging in tissues. In addition, RS delivers the full Raman spectrum of a molecule

and, therefore, it is a rather slow procedure; on the other hand, SRS and CARS provide a faster acquisition process as they only focus on a specific vibrational transition.

Surface enhanced Raman spectroscopy (SERS) provides enhanced signal exploiting the effects occurring near a metal surface, including metal nanoparticles, to produce electromagnetic and chemical amplification.[22] Limitations of SERS for biomedical applications depend on the knowledge of sensitive disease biomarkers and the availability of corresponding targeting molecules, as well as potential toxicity and the need for regulatory approval of the contrast agent.

Polarized Raman spectroscopy (PRS) provides information regarding both chemical composition and anisotropic response of highly oriented systems, like the amide I band of collagen and alpha helical structures with respect to the polarization angle of the incident laser light.

Spectral analysis

Spectral pre-processing

Due to the molecular complexity of biological samples, pre-processing steps of RS spectra are usually required to reduce noise, remove background, and normalize them to enable comparisons between data sets and gain diagnostic information. Autofluorescence is an intrinsic characteristic of biological specimens in optical spectroscopy. Autofluorescence is a consequence of irradiation of UV/Vis light of a specific wavelength upon biological specimen. Endogenous fluorophores contained in both cells and extracellular matrices are the major responsible of fluorescence emission. They are constituted by specific biochemical compounds contained in cells, namely amino acids, lipo-pigments along with pyridinic (NADPH) and flavin coenzymes and in extracellular matrix contained compound, such as collagen and elastin.[11]. Therefore, Raman spectra quality is affected by stochastic noise.[23] Specific algorithms performing a baseline-correction can help to subtract inelastic scatter fluorescence contribution.[24] Fourier filtering and polynomial curve fitting are also commonly used for baseline correction.[24,25] Morris *et al*.[26] showed that long-lived fluorescence signal could be prevented by applying time gating steps to the spectra acquisition procedure.

Spectral analysis and fingerprint identification

The multivariate analysis (supervised and non-supervised) is one of the most frequently used inquiry tools. Principal component analysis (PCA) represents the most common unsupervised method used for feature-extraction.[27-30] The number of dependent variables can be reduced to principal components (PCs) that are orthogonal and independent using PCA. Supervised methods can provide a label for the generated classes. Afterwards, the classes can be discriminated by a validation method. There are several alternatives for selection and extraction used in RS, including Fisher-based or correlation feature selection, multifactor dimensionality reduction and non-negative matrix factorization.[31-34]

Raman database

To date, free Raman spectra databases are only available for minerals, inorganic materials, or simple organic molecules. For examples, the Bio-Rad's SpectraBase (https://spectrabase.com) has over 24,000 spectra available, mostly of basic organic compounds.

Unfortunately, comprehensive databases of Raman spectra of biological compounds and tissues are still not available due to their complexity and the necessity of standardization of Raman data. Nevertheless, some reviews reported an extensive collection of most relevant Raman bands that can be found in a Raman tissue investigation. A review by Talari *et al*.[35] represents today the most complete list of assigned Raman peaks from biological specimens, reporting more than 1000 assigned bands extrapolated from Raman spectra from both healthy and pathological tissues. Other reviews are also helpful to assess comparison and attribution of the spectra from biological samples,[36] including lipids[37] and carbohydrates.[38]

RAMAN STUDIES OF SKELETAL TISSUES

Since Raman spectrum of H_2O is very weak and, therefore, does not interact with other molecular signals, RS has become a powerful tool for the analysis of biological samples.[12,39] Pioneering studies collected Raman spectra of proline oligomers and Poly-L-proline,[40] amino acids and Poly-L-hydroxyproline,[41] and of proteins and lysosomes in animal tissues *ex vivo*.[42] The first Raman report of bovine Achilles tendon showed the comparison in laser excitation scattering among gelatine, skin collagen (solid and solution

state) and constituent amino acids.[43] A few years later, RS was used for cells,[44] to discriminate live and dead cells,[45-47] and cell cycle or cell differentiation stages.[45,48-51] Over the past years, many studies were done on musculoskeletal tissues using various types of RS. Raman peaks characteristic for various musculoskeletal disorders, their biochemical assignment and relative literature references are reported in **Table 1**.

Tendon and ligaments

RS was long used to understand the structure of tendon and ligament proteins, such as collagen[43,52,53] and elastin.[43,54,55] More recently, studies focused on the analysis of collagen anisotropy and orientation in tendon by using PRS.[56,57] A dynamical insight into tendon molecular hierarchy adaptations to mechanical stress was provided by studying tendon collagen under strain. For this, multiscale approach was used, including Raman analysis of *in situ* loading test. Masic *et al*.[58] investigated cross-sectional area of rat tail tendon by combining confocal Raman microscopy and *in situ* stress-strain test.[56] They also investigated the role of water on collagen structure and mechanical behaviour with a combination of RS with X-ray diffraction, revealing tensile stress generated by conformation changes with water removal.[59] Using Fourier transform infrared (FT-IR) and confocal Raman microscopy, the adjustment of the collagen structure to tissue hydration was investigated.[60] In another study, spectra were obtained after rat tail tendon extension.[61] Spectral analysis provided features such as Raman shift position and Full Width Half Maximum of bands. When plotted as a function of the applied strain they showed that the 822 cm^{-1} band, representative of collagen backbone C–C, and 879 cm^{-1} band arising from carbonyl groups located at the side chain, respectively, decreased and increased with the applied strain. Collagen type I structure was also studied under hydrostatic pressure.[62]

The study of tendon enthesis by RS helped getting more insight on its development and structure.[63] Traditionally, it was believed that the tendon enthesis was divided into distinct regions, whereas mechanical studies suggested a gradual transition of tissue structure and functional properties. This latter tendon enthesis model was confirmed by Raman-based investigations, demonstrating that it is structured with a gradient of collagen and mineral components and crystallinity.[64-66] Raman spectral mapping of bone insertion of the anterior cruciate ligaments (ACL) and of rotator cuff tendon (RCT) revealed a similar

composition for the two structures, but with a different gradient of mineral content, which was higher for RCT.[67] These results provide the base for prosthetic engineers to accurately design specific biomaterials for the synthetic ligament. Likewise, the study by Marinovic *et al*. analysed the role of bone sialoprotein in the structure of the tendon enthesis,[68] revealing a regulatory role in the zone traditionally associated to the calcified fibrocartilage.

RS can be used as a tool to study tissue alterations associated to aging, pathologies, and disease treatments.[69,70] Rat tail tendons from adult and aged rats were studied by PRS and showed an increase in the anisotropy degree of Raman bands in tendons from old rats, therefore, a higher alignment of the collagen fibers can be associated to aged rat tissue.[69] In equine tendons, age-related changes in post-translational glycation of collagen were detected and likely correlated to decline in function.[70]

RS application has been described useful in the studies regarding experimental tendinitis,[71] tendon injuries,[72] or degenerative lesions of the supraspinatus RCT.[73] In the combined magnetic field, some studies dealt with periodontal ligament changes during orthodontic treatments[74,75] or in mandibular reconstruction.[76] Moreover, RS revealed useful in supporting the diagnostic of biochemical abnormalities of the ACL.[77] Schematic representation of *in vitro* musculoskeletal assessment conducted by PRS technique (as described in reference[69] is reported in **Figure 2. Figure 2A** shows a scheme of the PRS investigation performed on both old and adult rat tail tendon (RTT) fibres in order to assess the effect of ageing on the tissue. In **Figure 2B**, it is shown how collected spectra have been compared by age for each polarization direction. **Figure 2C** shows the anisotropy degree (Az) and (Ax) of different Raman Bands copared according to RTT age.

Cartilage and subchondral bone

Cartilage is principally composed of chondrocytes produced ECM, primarily consisting in water, type II collagen fibrils, proteoglycans, and hyaluronic acid. The cartilage is organized in three zones with different spatial organization, collagen and proteoglycans contents and orientation resulting in different mechanical and biological properties. Calcification of cartilage occurs to fix the collagen fibrils onto the adjacent bone (subchondral bone). The subchondral bone has the same composition as the cortical bone (see next paragraph).[78]

Raman spectra of healthy articular cartilage share several features with tendon and ligament spectra. Collagens represents the main component of both cartilaginous tissue and tendon. However, a band at ~1063 cm^{-1}, arising from the sulphated glycosaminoglycans (GAG), unique to cartilage, distinguishes its spectrum from that of other soft tissues and bone.[79,80] These observations using Raman technique were recently confirmed by fibre-based fluorescence lifetime (FL) technology allowing for real time study of the structural, compositional, and molecular contrast of cartilage.[81]

Osteoarthritis (OA) is a degenerative condition affecting articular cartilage and the whole joint, including the synovium and the osteochondral bone. In a preclinical rat model[82] and in clinical setups,[83] RS could distinguish between different OA severity grades. A RS analysis of synovial fluid from 40 patients with knee OA correlated with the pathology severity scores obtained using Kellgren/Lawrence (K/L) score which is based on X-rays analysis.[84] Cartilage calcification and water contents phenomenon also correlate with cartilage degeneration independently of age, and can be used as potential marker for early detection of joint degeneration.[85]

Changes in the water content in cartilage tissue is an early diagnostic of OA, and can help in the classification among different grades.[81,83,86] Among pathology spectra quality of cartilage was identified following distinct chemical fingerprint for the non-ochronotic, compared to ochronotic cartilage.[87] Moreover, it has been demonstrated that the progression of OA can be followed by evaluating chondrocyte differences using the amide I (1,612–1,696 cm^{-1}), amide III (1,229–1,300 cm^{-1}) and phenylalanine (1,001–1,007 cm^{-1}) bands; additionally OA progression is also correlated with a decrease of the nucleic acid content (780–794 cm^{-1} band).[88]

The biochemical composition of the ECM in the spongy and subchondral bone in patients with femoral neck fractures without osteopathic arthritis was examined,[5] demonstrating that Raman microspectroscopy can show alterations for osteopathic arthritis, characterized by relevant changes in hydroxyapatite (HA)-to-collagen ratio, carbonate apatite-to-HA ratio and disorganization in collagen secondary structure via amide III. SRS and CARS were used to analyse tissue microstructure in the region between calcified cartilage and subchondral bone, showing that cartilage microstructure differs

between regions subjected to different loadings in the deep areas, which might be important for mechanical interactions of cartilage and subchondral bone (**Fig. 3**).[89]

RS can be also used for the diagnosis of other joint pathologies, like gout, characterized by the deposition of monosodium urate in the joints and other organs. Through RS, it is possible to assess non-invasively (detecting through the skin) the presence of crystals situated around the first metatarsophalangeal joint.[84,90]

Bone

Bone is a multiscale mineralised tissue consisting of cortical bone, composed of highly structured and oriented osteon, and trabecular bone composed of interconnected trabecular rods.[91,92]

At the microscopic level, bone is a composite material containing an inorganic (mainly apatite crystals, calcium salts and water) and an organic phase comprising different types of cells from the mesenchymal and the hematopoietic lineages.[93] Giving access to the organic and inorganic components of bone, their composition, orientation, crystallinity and degree of crosslink, RS also gives access to bone quality and indirectly mechanical properties upon aging, diseases, or injuries and recoveries in a non or minimal invasive way.[94-96]

At the ultrastructural level, bone matrix is composed of type I collagen organised in mineralised collagen fibrils, further assembled in large collagen fibres.[97-99] The orientation and alignment of those collagen fibres together with the amount and quality of the inorganic phases contributes to the macrostructural organisation of bone tissue and, thus, to its mechanical properties. Giving access to information at the molecular level, RS enables the quantification of bone quality related parameters, such as minerals, matrix and their relative ratio, crystallinity, carbonate substitution, as well as collagen fibres primary and secondary structures.[98,100,101]

Photon migration into the bone and Raman signals arising from different depths of selected bones with various mineralization levels were analysed by SORS.[102] In other work, Raman signals were retrieved in depths up to about 5 mm, the penetration depth depending on the degree of bone mineralization. Besides, PRS gave access to the collagen fibril content, orientation, and crystallisation status of cortical bone, while spongy bone

was characterized up to the microstructural level, showing that the $\nu_1PO_4^{3-}$/amide I ratio, susceptible to polarization effect, brings information on collagen fibres orientation.[99,100,103]

Giving a quick access to bone mineral and organic components and, therefore, to biomechanical properties of bone,[94] RS also became a promising method for the detection of other bone and mineral related diseases, such as osteoporosis[96,104] and osteogenesis imperfecta.[105,106]

For the study of osteoporosis, Shu *et al*.[96] proposed the use of SORS in a transcutaneous approach to predict bone quality in a mouse model. Despite the overlay tissue interferences (mainly due to type I collagen), they demonstrated a strong correlation between bone quality metrics measured by Raman and detected by classical micro-CT, DXA and mechanical testing methods. Similarly, another study showed a strong correlation between bone mineral contents and fracture risks, but also and more importantly the involvement of the bone collagen components, essentially the amide I region of the Raman spectra.[104] SORS can detect subcortical tissue in the long bones of mice and rabbits and it is sensitive to biochemical changes in a mouse model with imperfect osteogenesis.[105] On the other hand, PRS revealed a correlation between mineral and collagen orientations and the mechanical phenotype of bones, while differences in composition alone failed to fully explain the differences in toughness between different disease genotypes.[107]

Fracture repair is a complex process involving many factors and steps aiming to restore the biological and mechanical function of bone.[108] If bone shows a high regenerative and healing capacity, fractures still fail to heal leading to delayed union or non-unions, and large bone defects. A better understanding of the healing course at all scales will enable the understanding of the possible causes of failures, crucial for the development of appropriate therapies or replacement strategies.[109] Many *in vitro* studies have been performed at the cellular level. In a subcritical rat calvaria defect, Ahamed *et al.* compared bone composition changes after 7 or 14 days healing period, and with intact bone [110]. RS data - i.e., the mineral matrix ratio ($\upsilon 1\ PO_4^{-3}$/ amide III, $\upsilon 1\ PO_4^{-3}$/ CH_2 wag), the carbonate/phosphate ratio, and the crystallinity corroborated with the *in vivo* callus formation stage. Recent studies investigated the application of the SORS to monitor bone healing *in vivo*.[102,111,112]. A schematic representation of *in vivo* clinical study carried out

using the SORS technique (as described in Dooley et al.[111]) is reported in **Figure 4**. Part (A) is a representation of bone healing process monitored *in vivo* by Spatially Offset Raman Spectroscopy (SORS). Intensity ratio of collagen and hydroxyapatite Raman bands can provide reliable information on healing process as a daily trend. In part (B) is reported the comparison of SORS spectra collected at different stage, of healing process, upon collagen:HA phantoms inserted in rat skulls. Different stages of bone regeneration are characterized by specific collagen:HA ratio.

Tissue engineered constructs for skeletal tissue repair

In case of natural tissue healing failure, autografts, allografts, or tissue engineered (TE) constructs are foreseen. In the three above mentioned musculoskeletal tissues (tendons, cartilage/subchondral bone, and bone), lifetime and success of the grafted material depend on its mechanical properties and rapid integration in native tissue. Typically, TE constructs comprise a scaffold showing specific requirements of the host tissue associated with tissue specific cells or stem cells aiming to restore structural, mechanical, and biological functionality of the injured tissue upon implantation. Major challenge in this field is the possibility to recapitulate the biological, mechanical, and structural composition of native tissue in an implantable construct. A successful clinical translation of TE constructs requires robust quality control prior to implantation and Good Laboratory Practices (GLP) certified fabrication procedures.

Cells. Autologous mesenchymal stromal cells (MSC) from bone marrow or adipose tissues are commonly used in TE constructs for bone, cartilage, or tendon repair. Being a heterogenous population, MSC differentiation and cell growth capacity differ among donors.[113] This lack of reproducibility, together with the difficulty to separate cell sub-populations, constitutes the main drawback to MSC clinical use. To date, cell characterization and subpopulation identification can only be assessed via methods, such as flow cytometry, gene expression analysis, immunocytochemistry; most of these methods involve the destruction of the original sample and are time consuming. As mentioned above in this review, RS showed the possibility to distinguish between live or dead cells,[46,47] as well as cells in different phases of their cycle.[45,48,49,51] In a recent publication, Rocha *et al*.[114] proposed RS to quantitatively characterise clonal MSC, and its use as a label-free biomolecular characterisation tool of MSC and sub-populations in a

mixed population. In this study, the authors created 4 immortalized cell lines out of 4 single-cells-derived colonies from an heterogenous cell population. Of those, 2 cell lines showed osteogenic, chondrogenic and adipogenic differentiation capacity (Y101, Y201), while the two other groups did not (Y102, Y202). Raman spectra analysis performed on the nuclear region of those cell subpopulations clearly showed signal discrepancies between the competent versus non-competent cell population as depicted by their overall Raman spectra (**Fig.5A**). Comparing the 4 MSC sub-populations to CD317 positive MSC (MSC positive control), or to dermal fibroblasts (MSC negative control, HDF), key differences mainly occurred at the protein (932 cm^{-1} band) and proteins DNA/RNA bands (971 cm^{-1}) but also in the region of the lipids, phospholipids, carbohydrates, and DNA/RNA region of the spectrum (1060 and 1085 cm^{-1}). Comparing the 4 MSC sub-populations (tri-lineage differentiation competent, or tri-lineage differentiation incompetent), main differences were observed in the protein region (932cm^{-1}), and the protein and DNA/RNA region (971 cm^{-1}). The authors further analysed the Raman spectra of the 4 different MSC cell lines comparing all peaks intensity between each other (Peak- Intensity-Ratio (PIR) analysis) and could discriminate between differentiation-competent cells and differentiation-incompetent cells. PIR panels that predominantly distinguish between those two groups of biological response were found in the DNA/RNA, carbohydrates, lipids and proteins (1060 cm^{-1}) (**Fig.5B**), and the protein, lipids, DNA/RNA region (1473 cm^{-1}) (**Fig.5C**)

Matrix. Cell differentiation phases can be monitored by analysing matrix deposition and mineralisation in contact with biomaterial surfaces.[49,115-118] Extracellular matrix (ECM) is a fundamental component of all living tissues; it is synthetised by tissue-specific cells and provides mechanical, structural, and biochemical support. Parallel to phenotype specific gene expression, ECM deposition is a key indicator of cell differentiation and a crucial factor in tissue integrity, repair, and the development of TE constructs. However, as for cell characterization, methods to analyse matrix deposition are mainly invasive, long-term, and time-consuming. Thus, the strength of using RS in TE relies on the possibility to conduct sample analysis directly at the ECM biomolecules level in a non-invasive way.

With the aim of monitoring changes in the properties of collagenous tissues, Shaik *et al*.[119] used several non-destructive techniques including Raman spectroscopy to monitor collagen digestion phases over time at the molecular level. Raman spectra intensity in the

region of the proline, hydroxyproline, C-Cα stretch and amide I region decreased over time. They also showed that with the longer digestion time (32h) type I collagen characteristic peaks (proline, amide III and C-Cα) disappeared, demonstrating the usability of RS in monitoring extra-cellular matrix proteins over time in the non-destructive manner.

The use of diffuse near infrared fibre-optic Raman spectra showed its efficacy in the analysis of TE cartilage constructs. Using this non-invasive approach, Bergholt *et al*. quantified the ECM components and showed a high correlation between RS output and classical biochemical assays for the measurement of collagen and GAGs (**Fig.6A**).[120] In a study published in 2018, Albro *et al*.[121] investigated the usability of RS in the characterisation TE cartilage constructs compared to native cartilage tissue. As shown in **Figure 6B**, Raman spectra obtained from TE constructs indicated similar protein contents to native cartilage, though Raman images calculated from the collagen and GAG Raman spectra, which depicted local heterogeneity between native and TE cartilage (**Fig.6C**).

Cell-Matrix interactions. Early cell-materials interactions are determinant for the further evolution of TE constructs. After sedimentation on a biomaterial surface, cells are sensing their environment in terms of chemistry, surface topography and stiffness, as well as possible added biological cues. Upon adhesion involving specific cell molecules, such as integrins, cells start to produce their own ECM promoting their growth, differentiation, further matrix deposition, and eventually matrix mineralisation, in the case of bone TE. Cell-material interactions are usually studied thought metabolic activity assays to assess cell viability and growth or using imaging techniques involving cell fixation and staining with antibodies. Recently, RS has shown the ability in monitoring the mineralization of bone nodules for *in vitro* bone TE applications. Cell differentiation can also be monitored upon matrix deposition and mineralisation in contact with biomaterial surfaces.[49,115-117] In a recent study, by combining classical RS spectra analysis, Raman spectral imaging, and mapping, Kalisz and co-workers could access not only to the biochemical changes at the interface between stem cells and osteo-inductive scaffolds, but also to the three-dimensional deposition of the ECM components and mineralization at the cell-material interface.[122] In their study, the authors first measured the Raman profiles of the three raw components (Chitosan (CHI), Beta 1,3 Glucan polysaccharide, and HA) they used in the fabrication of theirs scaffolds, and monitored the matrix deposited by MSCs from adipose

tissue and bone marrow (**Fig. 7**). The authors could identify molecular differences, spatial distribution, and relocalization between cell-seeded materials and raw materials (Amide I, II, and raw materials (CHI), Beta 1,3 HA) (**Fig. 7A**). They also could access to HA deposition and crystallinity along the ECM deposition by MSCs (**Fig. 7B**).

STATUS AND CHALLENGES FOR CLINICAL TRANSLATION

According to the most recent available literature concerning the musculoskeletal applications of RS, there are several proof-of-concept on preclinical studies, which might be translated into clinics. One of them regards the investigation of possible crystals like monosodium urate for gout, OA or rheumatoid arthritis, and calcium pyrophosphate in pseudogout in joint and synovial fluid using customized RS.[123,124]

RS can be used intra-operatively to improve surgical treatments for joint diseases or injuries.[80,125] Matsunaga *et al*.[77] reported the application of RS for the non-destructive diagnosis of molecular tissue degeneration, applied to *ex vivo* human ACL. Encouraging outcomes of this work could promote Raman microscopy as a reliable alternative to the invasive histology or to MRI, which is unable to identify the biochemical components related to degeneration.

A new method to address early diagnosis of OA was based on hydration status of cartilage assessment by RS, showing a non-destructive quantification of various water zones in cartilage, and calculation of up to 82% of the variance found in the permeability and combined modulus of articular cartilage.[86] Due to its simplicity and feasibility, this methodology can be used clinically during arthroscopy procedures to control cartilage consistency in a non-invasive or minimally invasive way with Raman probe. As well, the RS was adapted for arthroscopy of joint cadaveric knee tissues applying a custom-built fibre-optic probe.[80] Fibre-optic Raman spectra were compared to the reference spectra of cartilage, subchondral and cancellous bone collected by Raman microspectroscopy. This proof-of-concept study provided a basis for further development of arthroscopic Raman optical fibre probes for application in clinics.

During the last years, many works were published reporting the use of Raman-based tools for *in vivo* and intra-operative conditions.[126,127] However, for clinical translation, several requirements need to be fulfilled. In a nutshell, the general definition of standards for technical characteristics of Raman apparatus and for operative

parameters, and the use of a standard algorithm for real-time data analysis and interpretation are needed. Despite the existing literature showed that RS stands as a reliable and mature tool for clinical diagnosis and intraoperative procedure, to date no specific reports or ISOs for the clinical use of RS based tools or procedures are available. These issues triggered a large-scale cross-laboratory study,[128] involving 35 different spectroscopic devices Europe-wide. This study aimed to define how different measurement conditions and experimental setups can affect the quality and differences of Raman spectra, focusing on the four most important metrics defining Raman profiles: peak width, peak shift, signal-to-noise ratio, and specific peak ratios. Authors concluded that the standardization of these parameters is a fundamental step for the definition of a common steppingstone to move RS from laboratories toward real-life application, such as RS use as bioanalytical protocol for clinical applications.

CONCLUSION

In conclusion, RS represents an important tool and has a great clinical potential in the examination of the musculoskeletal system. It provides deeper insights into comprehensive molecular composition of tissues through *in situ*, label-free and non-destructive measurements, paving a new way in the life sciences. Furthermore, Raman probe microscopy associated with chemometric-generated hyperspectral imaging can provide a real-time, augmented visualization of the region of interest, allowing for fast recognition and distinction of tissues and their biochemical status.

ACKNOWLEDGMENTS

The research of the authors affiliated to AO Research Institute Davos is supported by the AO Foundation.

AUTHORSHIP CONFIRMATION STATEMENT

Marco Fosca: writing, figures preparation, reviewing, editing. Valentina Basoli: writing, figures preparation, reviewing, editing. Elena Della Bella: writing, figures preparation, reviewing, editing. Fabrizio Russo: writing, reviewing. Gianluca Vadalà: reviewing, editing. Mauro Alini: reviewing, editing. Julietta V. Rau: writing, reviewing, editing. Sophie Verrier: writing, reviewing, figures preparation, editing. All authors agreed to submit this review article.

DISCLOSURE STATEMENT

No competing financial interests exist.

REFERENCES

1. Cieza A, Causey K, Kamenov K, Hanson SW, Chatterji S, Vos T. Global estimates of the need for rehabilitation based on the Global Burden of Disease study 2019: a systematic analysis for the Global Burden of Disease Study 2019. The Lancet 2020;396:2006-2017.

2. Kumamoto Y, Harada Y, Takamatsu T, Tanaka H. Label-free molecular imaging and analysis by Raman spectroscopy. Acta histochemica et cytochemica 2018;51:101-110.

3. Raman CV, Krishnan KS. A new type of secondary radiation. Nature 1928;121:501-502.

4. Yin N-H, Parker AW, Matousek P, Birch HL. Detection of Age-Related Changes in Tendon Molecular Composition by Raman Spectroscopy—Potential for Rapid, Non-Invasive Assessment of Susceptibility to Injury. International journal of molecular sciences 2020;21:2150.

5. Buchwald T, Niciejewski K, Kozielski M, Szybowicz M, Siatkowski M, Krauss H. Identifying compositional and structural changes in spongy and subchondral bone from the hip joints of patients with osteoarthritis using Raman spectroscopy. J Biomed Opt 2012;17:017007.

6. Pezzotti G, Rondinella A, Marin E, et al. Raman spectroscopic investigation on the molecular structure of apatite and collagen in osteoporotic cortical bone. Journal of the mechanical behavior of biomedical materials 2017;65:264-273.

7. Buckley K, Kerns JG, Vinton J, et al. Towards the in vivo prediction of fragility fractures with Raman spectroscopy. Journal of Raman Spectroscopy 2015;46:610-618.

8. Takahashi Y, Sugano N, Takao M, Sakai T, Nishii T, Pezzotti G. Raman spectroscopy investigation of load-assisted microstructural alterations in human knee cartilage: preliminary study into diagnostic potential for osteoarthritis. Journal of the mechanical behavior of biomedical materials 2014;31:77-85.

9. Shaikh R, Nippolainen E, Virtanen V, et al. Raman spectroscopy is sensitive to biochemical changes related to various cartilage injuries. Journal of Raman Spectroscopy 2021;52:796-804.

10. Georgakoudi I, Rice WL, Hronik-Tupaj M, Kaplan DL. Optical spectroscopy and imaging for the noninvasive evaluation of engineered tissues. Tissue Eng Part B Rev 2008;14:321-340.

11. Monici M. Cell and tissue autofluorescence research and diagnostic applications. *Biotechnology Annual Review*: Elsevier; 2005. pp. 227-256.

12. Pappas D, Smith BW, Winefordner JD. Raman spectroscopy in bioanalysis. Talanta 2000;51:131-144.

13. Mahadevan-Jansen A, Mitchell MF, Ramanujam N, Utzinger U, Richards-Kortum R. Development of a fiber optic probe to measure NIR Raman spectra of cervical tissue in vivo. Photochem Photobiol 1998;68:427-431.

14. Jermyn M, Mok K, Mercier J, et al. Intraoperative brain cancer detection with Raman spectroscopy in humans. Sci Transl Med 2015;7:274ra219.

15. Wang J, Bergholt MS, Zheng W, Huang Z. Development of a beveled fiber-optic confocal Raman probe for enhancing in vivo epithelial tissue Raman measurements at endoscopy. Opt Lett 2013;38:2321-2323.

16. Wood JJ, Kendall C, Hutchings J, et al. Evaluation of a confocal Raman probe for pathological diagnosis during colonoscopy. Colorectal Dis 2014;16:732-738.

17. Stone N, Baker R, Rogers K, Parker AW, Matousek P. Subsurface probing of calcifications with spatially offset Raman spectroscopy (SORS): future possibilities for the diagnosis of breast cancer. Analyst 2007;132:899-905.

18. Keller MD, Majumder SK, Mahadevan-Jansen A. Spatially offset Raman spectroscopy of layered soft tissues. Opt Lett 2009;34:926-928.

19. Schulmerich MV, Cole JH, Dooley KA, et al. Noninvasive Raman tomographic imaging of canine bone tissue. J Biomed Opt 2008;13:020506.

20. Liu W, Ong YH, Yu XJ, et al. Snapshot depth sensitive Raman spectroscopy in layered tissues. Optics Express 2016;24:28312-28325.

21. Alfonso-Garcia A, Mittal R, Lee ES, Potma EO. Biological imaging with coherent Raman scattering microscopy: a tutorial. J Biomed Opt 2014;19:71407.

22. Schlucker S. Surface-enhanced Raman spectroscopy: concepts and chemical applications. Angew Chem Int Ed Engl 2014;53:4756-4795.

23. Smulko JM, Dingari NC, Soares JS, Barman I. Anatomy of noise in quantitative biological Raman spectroscopy. Bioanalysis 2014;6:411-421.

24. Schulze G, Jirasek A, Yu MM, Lim A, Turner RF, Blades MW. Investigation of selected baseline removal techniques as candidates for automated implementation. Appl Spectrosc 2005;59:545-574.

25. Zhao J, Lui H, McLean DI, Zeng H. Automated autofluorescence background subtraction algorithm for biomedical Raman spectroscopy. Appl Spectrosc 2007;61:1225-1232.

26. Morris MD, Matousek P, Towrie M, Parker AW, Goodship AE, Draper ER. Kerr-gated time-resolved Raman spectroscopy of equine cortical bone tissue. J Biomed Opt 2005;10:14014.

27. Li Y, Pan J, Chen G, et al. Micro-Raman spectroscopy study of cancerous and normal nasopharyngeal tissues. J Biomed Opt 2013;18:27003.

28. Rau JV, Graziani V, Fosca M, et al. RAMAN spectroscopy imaging improves the diagnosis of papillary thyroid carcinoma. Sci Rep 2016;6:35117.

29. Palermo A, Fosca M, Tabacco G, et al. Raman Spectroscopy Applied to Parathyroid Tissues: A New Diagnostic Tool to Discriminate Normal Tissue from Adenoma. Anal Chem 2018;90:847-854.

30. Rau JV, Marini F, Fosca M, Cippitelli C, Rocchia M, Di Napoli A. Raman spectroscopy discriminates malignant follicular lymphoma from benign follicular hyperplasia and from tumour metastasis. Talanta 2019;194:763-770.

31. Hall MA, Smith LA. Feature Selection for Machine Learning: Comparing a Correlation-Based Filter Approach to the Wrapper. presented at the FLAIRS conference, 1999.

32. Dhillon IS, Sra S. Generalized nonnegative matrix approximations with Bregman divergences. presented at the NIPS, 2005.

33. Fenn MB, Pappu V, Georgeiv PG, Pardalos PM. Raman spectroscopy utilizing Fisher-based feature selection combined with Support Vector Machines for the characterization of breast cell lines. Journal of Raman Spectroscopy 2013;44:939-948.

34. Zhang BH, Jiang YC, Sha W, Zhang XY, Cui ZF. [Quantitative analysis of thiram by surface-enhanced raman spectroscopy combined with feature extraction Algorithms]. Guang Pu Xue Yu Guang Pu Fen Xi 2015;35:390-393.

35. Talari ACS, Movasaghi Z, Rehman S, Rehman IU. Raman Spectroscopy of Biological Tissues. Applied Spectroscopy Reviews 2015;50:46-111.

36. Rygula A, Majzner K, Marzec KM, Kaczor A, Pilarczyk M, Baranska M. Raman spectroscopy of proteins: a review. Journal of Raman Spectroscopy 2013;44:1061-1076.

37. Czamara K, Majzner K, Pacia MZ, Kochan K, Kaczor A, Baranska M. Raman spectroscopy of lipids: a review. Journal of Raman Spectroscopy 2015;46:4-20.

38. Wiercigroch E, Szafraniec E, Czamara K, et al. Raman and infrared spectroscopy of carbohydrates: A review. Spectrochim Acta A Mol Biomol Spectrosc 2017;185:317-335.

39. Butler HJ, Ashton L, Bird B, et al. Using Raman spectroscopy to characterize biological materials. Nat Protoc 2016;11:664-687.

40. Rippon WB, Koenig JL, Walton AG. Raman spectroscopy of proline oligomers and poly-L-proline. J Am Chem Soc 1970;92:7455-7459.

41. Deveney MJ, Walton AG, Koenig JL. Raman spectra of imino acids and poly-L-hydroxyproline. Biopolymers 1971;10:615-630.

42. Lord RC, Yu NT. Laser-excited Raman spectroscopy of biomolecules. I. Native lysozyme and its constituent amino acids. J Mol Biol 1970;50:509-524.

43. Frushour BG, Koenig JL. Raman scattering of collagen, gelatin, and elastin. Biopolymers 1975;14:379-391.

44. Puppels GJ, de Mul FF, Otto C, et al. Studying single living cells and chromosomes by confocal Raman microspectroscopy. Nature 1990;347:301-303.

45. I.Notingher, J.R.Jones, S.Verrier, et al. Application of FTIR and RAMAN spectroscopy to characterisation of bioactive materials and living cells. Spectrosc Int J 2003;17:275-288.

46. Verrier S, Notingher I, Polak JM, Hench LL. In situ monitoring of cell death using Raman microspectroscopy. Biopolymers 2004;74:157-162.

47. Verrier S, Zoladek A, Notingher I. Raman micro-spectroscopy as a non-invasive cell viability test. Methods Mol Biol 2011;740:179-189.

48. Germond A, Ichimura T, Chiu LD, Fujita K, Watanabe TM, Fujita H. Cell type discrimination based on image features of molecular component distribution. Sci Rep 2018;8:11726.

49. Kunstar A, Leferink AM, Okagbare PI, et al. Label-free Raman monitoring of extracellular matrix formation in three-dimensional polymeric scaffolds. J R Soc Interface 2013;10:20130464.

50. Rice WL, Kaplan DL, Georgakoudi I. Quantitative biomarkers of stem cell differentiation based on intrinsic two-photon excited fluorescence. J Biomed Opt 2007;12:060504.

51. Rice WL, Kaplan DL, Georgakoudi I. Two-photon microscopy for non-invasive, quantitative monitoring of stem cell differentiation. PLoS One 2010;5:e10075.

52. Reiser KM, McCourt AB, Yankelevich DR, Knoesen A. Structural origins of chiral second-order optical nonlinearity in collagen: amide I band. Biophys J 2012;103:2177-2186.

53. Kerns JG, Buckley K, Churchwell J, Parker AW, Matousek P, Goodship AE. Is the Collagen Primed for Mineralization in Specific Regions of the Turkey Tendon? An Investigation of the Protein-Mineral Interface Using Raman Spectroscopy. Anal Chem 2016;88:1559-1563.

54. Green E, Ellis R, Winlove P. The molecular structure and physical properties of elastin fibers as revealed by Raman microspectroscopy. Biopolymers 2008;89:931-940.

55. Prescott B, Renugopalakrishnan V, Thomas GJ, Jr. Raman spectrum and structure of elastin in relation to type-II beta-turns. Biopolymers 1987;26:934-936.

56. Janko M, Davydovskaya P, Bauer M, Zink A, Stark RW. Anisotropic Raman scattering in collagen bundles. Opt Lett 2010;35:2765-2767.

57. Galvis L, Dunlop JW, Duda G, Fratzl P, Masic A. Polarized Raman anisotropic response of collagen in tendon: towards 3D orientation mapping of collagen in tissues. PLoS One 2013;8:e63518.

58. Masic A, Bertinetti L, Schuetz R, et al. Observations of multiscale, stress-induced changes of collagen orientation in tendon by polarized Raman spectroscopy. Biomacromolecules 2011;12:3989-3996.

59. Masic A, Bertinetti L, Schuetz R, et al. Osmotic pressure induced tensile forces in tendon collagen. Nat Commun 2015;6:5942.

60. Ribeiro AR, Barbaglio A, Oliveira MJ, et al. Correlations between the biochemistry and mechanical states of a sea-urchin ligament: a mutable collagenous structure. Biointerphases 2012;7:38.

61. Wang YN, Galiotis C, Bader DL. Determination of molecular changes in soft tissues under strain using laser Raman microscopy. Journal of Biomechanics 2000;33:483-486.

62. Paschou AM, Katsikini M, Christofilos D, Arvanitidis J, Ves S. High pressure Raman study of type-I collagen. FEBS J 2018;285:2641-2653.

63. Schwartz AG, Lipner JH, Pasteris JD, Genin GM, Thomopoulos S. Muscle loading is necessary for the formation of a functional tendon enthesis. Bone 2013;55:44-51.

64. Wopenka B, Kent A, Pasteris JD, Yoon Y, Thomopoulos S. The tendon-to-bone transition of the rotator cuff: a preliminary Raman spectroscopic study documenting the gradual mineralization across the insertion in rat tissue samples. Appl Spectrosc 2008;62:1285-1294.

65. Genin GM, Kent A, Birman V, et al. Functional grading of mineral and collagen in the attachment of tendon to bone. Biophys J 2009;97:976-985.

66. Schwartz AG, Pasteris JD, Genin GM, Daulton TL, Thomopoulos S. Mineral distributions at the developing tendon enthesis. PLoS One 2012;7:e48630.

67. Wu Y, Dong Y, Jiang J, Li H, Zhu T, Chen S. Evaluation of the Bone-ligament and tendon insertions based on Raman spectrum and its PCA and CLS analysis. Sci Rep 2017;7:38706.

68. Marinovich R, Soenjaya Y, Wallace GQ, et al. The role of bone sialoprotein in the tendon-bone insertion. Matrix Biol 2016;52-54:325-338.

69. Van Gulick L, Saby C, Morjani H, Beljebbar A. Age-related changes in molecular organization of type I collagen in tendon as probed by polarized SHG and Raman microspectroscopy. Sci Rep 2019;9:7280.

70. Yin NH, Parker AW, Matousek P, Birch HL. Detection of Age-Related Changes in Tendon Molecular Composition by Raman Spectroscopy-Potential for Rapid, Non-Invasive Assessment of Susceptibility to Injury. Int J Mol Sci 2020;21:2150.

71. de Carvalho PK, Silveira L, Jr., Barbosa D, Munin E, Salgado MA, Villaverde AB. Analysis of experimental tendinitis in rats treated with laser and platelet-rich plasma therapies by Raman spectroscopy and histometry. Lasers Med Sci 2016;31:19-26.

72. Moura Junior Mde J, Maia Filho AL, Pessoa DR, et al. Assessing the biochemical changes of tendons of rats in an experimental model of tenotomy under therapeutic ultrasound and LEDs (625 and 945 nm) by near-infrared Raman spectroscopy. Lasers Med Sci 2015;30:1729-1738.

73. Penteado SC, Fogazza BP, Carvalho Cda S, et al. Diagnosis of degenerative lesions of supraspinatus rotator cuff tendons by Fourier transform-Raman spectroscopy. J Biomed Opt 2008;13:014018.

74. Camerlingo C, d'Apuzzo F, Grassia V, Perillo L, Lepore M. Micro-Raman spectroscopy for monitoring changes in periodontal ligaments and gingival crevicular fluid. Sensors (Basel) 2014;14:22552-22563.

75. Perillo L, d'Apuzzo F, Illario M, et al. Monitoring Biochemical and Structural Changes in Human Periodontal Ligaments during Orthodontic Treatment by Means of Micro-Raman Spectroscopy. Sensors (Basel) 2020;20:

76. Wang L, Su YX, Zheng GS, Liao GQ, Zhang WH. Healing masseter entheses of mandibular reconstruction with autograft--Raman spectroscopic and histological study. Int J Oral Maxillofac Surg 2013;42:915-922.

77. Matsunaga R, Takahashi Y, Takahashi RH, et al. A new method for diagnosing biochemical abnormalities of anterior cruciate ligament (ACL) in human knees: A Raman spectroscopic study. Acta Biomater 2019;99:284-294.

78. Buckwalter JA, Mankin HJ, Grodzinsky AJ. Articular cartilage and osteoarthritis. Instructional Course Lectures-American Academy of Orthopaedic Surgeons 2005;54:465.

79. Beek JF, Blokland P, Posthumus P, et al. In vitro double-integrating-sphere optical properties of tissues between 630 and 1064 nm. Phys Med Biol 1997;42:2255-2261.

80. Esmonde-White KA, Esmonde-White FW, Morris MD, Roessler BJ. Fiber-optic Raman spectroscopy of joint tissues. Analyst 2011;136:1675-1685.

81. Lagarto JL, Shcheslavskiy V, Saverio Pavone F, Cicchi R. Simultaneous fluorescence lifetime and Raman fiber-based mapping of tissues. Opt Lett 2020;45:2247-2250.

82. de Souza RA, Xavier M, Mangueira NM, et al. Raman spectroscopy detection of molecular changes associated with two experimental models of osteoarthritis in rats. Lasers in medical science 2014;29:797-804.

83. Kumar R, Grønhaug KM, Afseth NK, et al. Optical investigation of osteoarthritic human cartilage (ICRS grade) by confocal Raman spectroscopy: a pilot study. Analytical and bioanalytical chemistry 2015;407:8067-8077.

84. Esmonde-White KA, Mandair GS, Raaii F, et al. Raman spectroscopy of synovial fluid as a tool for diagnosing osteoarthritis. Journal of biomedical optics 2009;14:034013.

85. Hawellek T, Hubert J, Hischke S, et al. Calcification of the acetabular labrum of the hip: prevalence in the general population and relation to hip articular cartilage and fibrocartilage degeneration. Arthritis research & therapy 2018;20:1-10.

86. Unal M, Akkus O, Sun J, et al. Raman spectroscopy-based water content is a negative predictor of articular human cartilage mechanical function. Osteoarthritis Cartilage 2019;27:304-313.

87. Taylor AM, Jenks DD, Kammath VD, et al. Raman Spectroscopy identifies differences in ochronotic and non-ochronotic cartilage; a potential novel technique for monitoring ochronosis. Osteoarthritis and cartilage 2019;27:1244-1251.

88. Kumar R, Singh GP, Gronhaug KM, et al. Single cell confocal Raman spectroscopy of human osteoarthritic chondrocytes: a preliminary study. Int J Mol Sci 2015;16:9341-9353.

89. Mansfield J, Moger J, Green E, Moger C, Winlove CP. Chemically specific imaging and in-situ chemical analysis of articular cartilage with stimulated Raman scattering. J Biophotonics 2013;6:803-814.

90. Curran DJ, Rubin L, Towler MR. Raman spectroscopy applied to the noninvasive detection of monosodium urate crystal deposits. Clinical Medicine Insights: Arthritis and Musculoskeletal Disorders 2015;8:CMAMD. S29061.

91. Boskey AL, Posner AS. Bone structure, composition, and mineralization. Orthop Clin North Am 1984;15:597-612.

92. Boskey AL, Mendelsohn R. Infrared spectroscopic characterization of mineralized tissues. Vib Spectrosc 2005;38:107-114.

93. Feng X. Chemical and Biochemical Basis of Cell-Bone Matrix Interaction in Health and Disease. Curr Chem Biol 2009;3:189-196.

94. Mandair GS, Morris MD. Contributions of Raman spectroscopy to the understanding of bone strength. Bonekey Rep 2015;4:620.

95. Morris MD, Mandair GS. Raman assessment of bone quality. Clin Orthop Relat Res 2011;469:2160-2169.

96. Shu C, Chen K, Lynch M, Maher JR, Awad HA, Berger AJ. Spatially offset Raman spectroscopy for in vivo bone strength prediction. Biomed Opt Express 2018;9:4781-4791.

97. Smith JW. Collagen fibre patterns in mammalian bone. J Anat 1960;94:329-344.

98. Li Y, Aparicio C. Discerning the subfibrillar structure of mineralized collagen fibrils: a model for the ultrastructure of bone. PLoS One 2013;8:e76782.

99. Toledano M, Toledano-Osorio M, Guerado E, Caso E, Aguilera FS, Osorio R. Biochemical assessment of nanostructures in human trabecular bone: Proposal of a Raman microspectroscopy based measurements protocol. Injury 2018;49 Suppl 2:S11-s21.

100. Falgayrac G, Facq S, Leroy G, Cortet B, Penel G. New method for Raman investigation of the orientation of collagen fibrils and crystallites in the Haversian system of bone. Appl Spectrosc 2010;64:775-780.

101. Georgiadis M, Müller R, Schneider P. Techniques to assess bone ultrastructure organization: orientation and arrangement of mineralized collagen fibrils. J R Soc Interface 2016;13:

102. Sowoidnich K, Churchwell JH, Buckley K, Goodship AE, Parker AW, Matousek P. Spatially offset Raman spectroscopy for photon migration studies in bones with different mineralization levels. Analyst 2017;142:3219-3226.

103. Kozielski M, Buchwald T, Szybowicz M, Błaszczak Z, Piotrowski A, Ciesielczyk B. Determination of composition and structure of spongy bone tissue in human head of femur by Raman spectral mapping. J Mater Sci Mater Med 2011;22:1653-1661.

104. Inzana JA, Maher JR, Takahata M, Schwarz EM, Berger AJ, Awad HA. Bone fragility beyond strength and mineral density: Raman spectroscopy predicts femoral fracture toughness in a murine model of rheumatoid arthritis. J Biomech 2013;46:723-730.

105. Feng G, Ochoa M, Maher JR, Awad HA, Berger AJ. Sensitivity of spatially offset Raman spectroscopy (SORS) to subcortical bone tissue. J Biophotonics 2017;10:990-996.

106. Kozloff KM, Carden A, Bergwitz C, et al. Brittle IV mouse model for osteogenesis imperfecta IV demonstrates postpubertal adaptations to improve whole bone strength. J Bone Miner Res 2004;19:614-622.

107. Makowski AJ, Pence IJ, Uppuganti S, et al. Polarization in Raman spectroscopy helps explain bone brittleness in genetic mouse models. J Biomed Opt 2014;19:117008.

108. Verrier S, Alini M, Alsberg E, et al. Tissue engineering and regenerative approaches to improving the healing of large bone defects. Eur Cell Mater 2016;32:87-110.

109. Casanova M, Schindeler A, Little D, Müller R, Schneider P. Quantitative phenotyping of bone fracture repair: a review. Bonekey Rep 2014;3:550.

110. Ahmed R, Law AWL, Cheung TW, Lau C. Raman spectroscopy of bone composition during healing of subcritical calvarial defects. Biomed Opt Express 2018;9:1704-1716.

111. Dooley M, McLaren J, Rose F, Notingher I. Investigating the feasibility of spatially offset Raman spectroscopy for in-vivo monitoring of bone healing in rat calvarial defect models. J Biophotonics 2020;e202000190.

112. Dooley M, Prasopthum A, Liao Z, et al. Spatially-offset Raman spectroscopy for monitoring mineralization of bone tissue engineering scaffolds: feasibility study based on phantom samples. Biomed Opt Express 2019;10:1678-1690.

113. Herrmann M, Hildebrand M, Menzel U, et al. Phenotypic Characterization of Bone Marrow Mononuclear Cells and Derived Stromal Cell Populations from Human Iliac Crest, Vertebral Body and Femoral Head. Int J Mol Sci 2019;20:

114. Rocha RA, Fox JM, Genever PG, Hancock Y. Biomolecular phenotyping and heterogeneity assessment of mesenchymal stromal cells using label-free Raman spectroscopy. Sci Rep 2021;11:4385.

115. Brauchle E, Carvajal Berrio D, Rieger M, Schenke-Layland K, Reinert S, Alexander D. Raman Spectroscopic Analyses of Jaw Periosteal Cell Mineralization. Stem Cells Int 2017;2017:1651376.

116. Ghita A, Pascut FC, Sottile V, Notingher I. Monitoring the mineralisation of bone nodules in vitro by space- and time-resolved Raman micro-spectroscopy. Analyst 2014;139:55-58.

117. Jell G, Notingher I, Tsigkou O, et al. Bioactive glass-induced osteoblast differentiation: a noninvasive spectroscopic study. J Biomed Mater Res A 2008;86:31-40.

118. Maquet V, Boccaccini AR, Pravata L, Notingher I, Jérôme R. Porous poly(alpha-hydroxyacid)/Bioglass composite scaffolds for bone tissue engineering. I: Preparation and in vitro characterisation. Biomaterials 2004;25:4185-4194.

119. Shaik TA, Lagarto JL, Baria E, et al. Monitoring Changes in Biochemical and Biomechanical Properties of Collagenous Tissues Using Label-Free and Nondestructive Optical Imaging Techniques. Analytical Chemistry 2021;93:3813-3821.

120. Bergholt MS, Albro MB, Stevens MM. Online quantitative monitoring of live cell engineered cartilage growth using diffuse fiber-optic Raman spectroscopy. Biomaterials 2017;140:128-137.

121. Albro MB, Bergholt MS, St-Pierre JP, et al. Raman spectroscopic imaging for quantification of depth-dependent and local heterogeneities in native and engineered cartilage. NPJ Regen Med 2018;3:3.

122. Kalisz G, Przekora A, Kazimierczak P, et al. Application of Raman Spectroscopic Imaging to Assess the Structural Changes at Cell-Scaffold Interface. Int J Mol Sci 2021;22:

123. Cheng X, Haggins DG, York RH, Yeni YN, Akkus O. Analysis of crystals leading to joint arthropathies by Raman spectroscopy: comparison with compensated polarized imaging. Appl Spectrosc 2009;63:381-386.

124. Li B, Yang S, Akkus O. A customized Raman system for point-of-care detection of arthropathic crystals in the synovial fluid. Analyst 2014;139:823-830.

125. Pezzotti G, Sugano N. Cartilage Regeneration and the Role of Vibrational Spectroscopy in Future Joint Arthroplasty. Key Engineering Materials 2013;541:121-133.

126. DePaoli D, Goetz L, Gagnon D, et al. Intraoperative fiber optic guidance during chronic electrode implantation in deep brain stimulation neurosurgery: proof of concept in primates. J Neurosurg 2019;132:1810-1819.

127. Desroches J, Lemoine E, Pinto M, et al. Development and first in-human use of a Raman spectroscopy guidance system integrated with a brain biopsy needle. J Biophotonics 2019;12:e201800396.

128. Guo S, Beleites C, Neugebauer U, et al. Comparability of Raman Spectroscopic Configurations: A Large Scale Cross-Laboratory Study. Anal Chem 2020;92:15745-15756.

TABLES

Table 1: Outline of various Raman Spectroscopy derived techniques presented in this work. Most relevant Raman bands and their assignments related to specific musculoskeletal disorders corresponding literature refences are reported.

Raman technique	**Raman shift position (cm^{-1})**	**Assignment**	**Skeletal disorder**	**Reference**
RS	800–950	tyrosine, proline, and hydroxyproline	tendinitis, tendon injuries	71,72
	1006	phenylalanine/tryptophan		
	1250–1350	amide III and CH modes		
	1454, 1670	CH_3/CH_2 bending and amide I		
	962	hydroxyapatite	osteoarthritis	82
	1, 1280	amide III		
	1070	carbonate		
	1220-1360	amide III		125
	1450, 2840-2986	C-H bond		
	1600-1720	amide I		
	1500-1700	CN CC, C—N, amide I vibrational bands of DNA, RNA, phenylalanine, tyrosine,	degenerative lesions of the supraspinatus rotator cuff tear	73

	588, 628, 686, and 1503	monosodium urate	gout	90
	1070	carbonate	osteogenesis imperfecta	106
	960	hydroxyapatite		
	1675	amide I		
SORS	962	hydroxyapatite	osteoporosis	96
	1070	carbonate		
	1250	amide III		
	1450	CH_2 wag		
	1665	amide I		
	960	hydroxyapatite	osteogenesis imperfecta	105
	1450	CH_2 wag		
	1650	amide I		
	961	phosphate	mineralization level (due to general disorder)	102
	1071	carbonate substitution		
	1450	CH_2 deformation band		
PRS	1250	amide III	tendon stress strain test	58
	1450	C—H bending		
	1665	C═O stretching of the protein backbone		
	937	collagen backbone	tendon ageing	69

	960	hydroxyapatite		
	1665	amide I secondary protein structures		
	853, 934	proline		70
	904	collagen backbone		
	990, 1003	phenylalanine		
	1100	ring-associated and carbohydrate bands		
	1400–1500	CH_2 bending		
	430, 590, 960	phosphate	bone brittleness	107
	857, 878	proline, hydroxyproline		
	1074	carbonate		
	1248	amide III		
	1668	amide I		
micro-Raman	1200-1300	amide III	periodontal ligaments changes during orthodontic treatment	74,75
	1620-1680	amide I		
	2930	CH_3 modes		
	960	hydroxyapatite	masseter entheses of mandibular	76
	2940, 1003	type I collagen		

			reconstruction	
	784	DNA/RNA	biochemical abnormalities of anterior cruciate ligament	77
	1002, 1030	phenylalanine		
	1101	Isomer conformation in lipids		
	1516	C═C bond stretching mode (carotenoids)		
	1749	phospholipids		
	962	hydroxyapatite	osteoarthritis	83,87
	1003	phenylalanine		
	1064	proteoglycan		
	1070	carbonate		
	1280	amide III		
CARS	960	hydroxyapatite	osteoarthritis	89

FIGURE LEGENDS

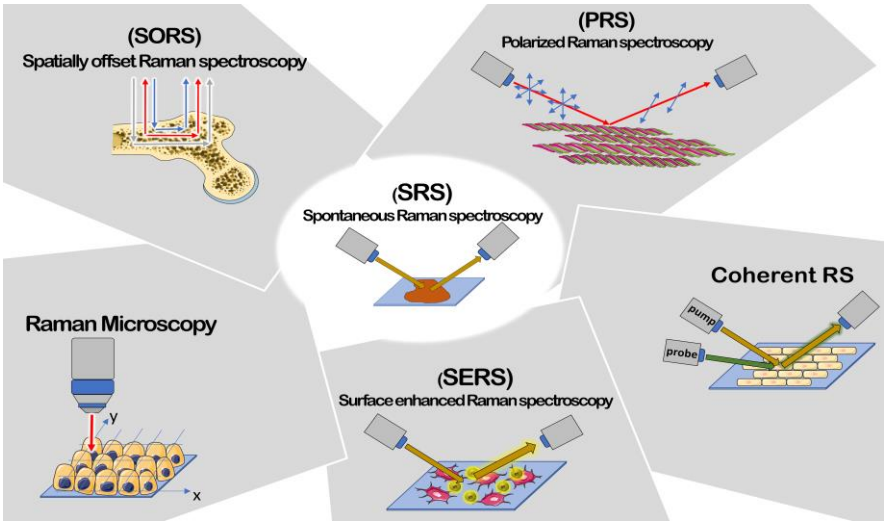

Figure 1: Summary of Raman spectroscopy techniques. Polarized Raman Spectroscopy (PRS) suitable for anisotropic systems; Raman Microscopy, able to perform correlation between chemical and morphological features; Spatially Offset Raman Spectroscopy (SORS) for deep regions signal's collection; Coherent Raman Spectroscopy (SRS & CARS) characterized by an improvement in signal intensity (up to 10^5 factor) and a faster acquisition; Surface Enhanced Raman Spectroscopy (SERS) characterized by signal intensity enhancement up to 10^{10} factor due to plasmonic effect between metal particles and sample.

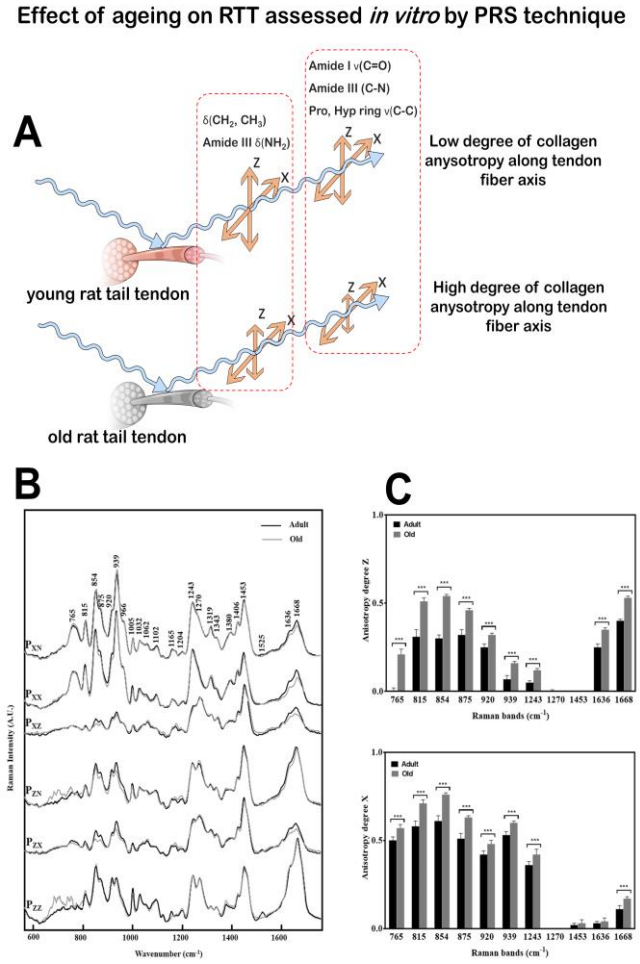

Figure 2: Raman spectroscopy for the analysis of tendon ageing. (A) Schematic representation of the effect of ageing on rat tail tendon (RTT) by Polarized Raman Spectroscopy (PRS). (B) Mean conventional and PRS spectra measured on adult (black line) and old (grey line) RTT with the same experimental conditions and compared according to the age. (C) polarization anisotropy (Az) and (Ax) calculated on specific collagen bands from adult (black bar) and old (grey bar) RTT. Intensity ratio of different Raman bands can provide anisotropy degree of collagen backbone along tendon fibre axis. A higher degree of anisotropy characterized old-aged tendon in comparison to the young one. Figures in panels (B) and (C) are adapted with permission from Van Gulick *et al*. (doi.org/10.1038/s41598-019-43636-2).[69]

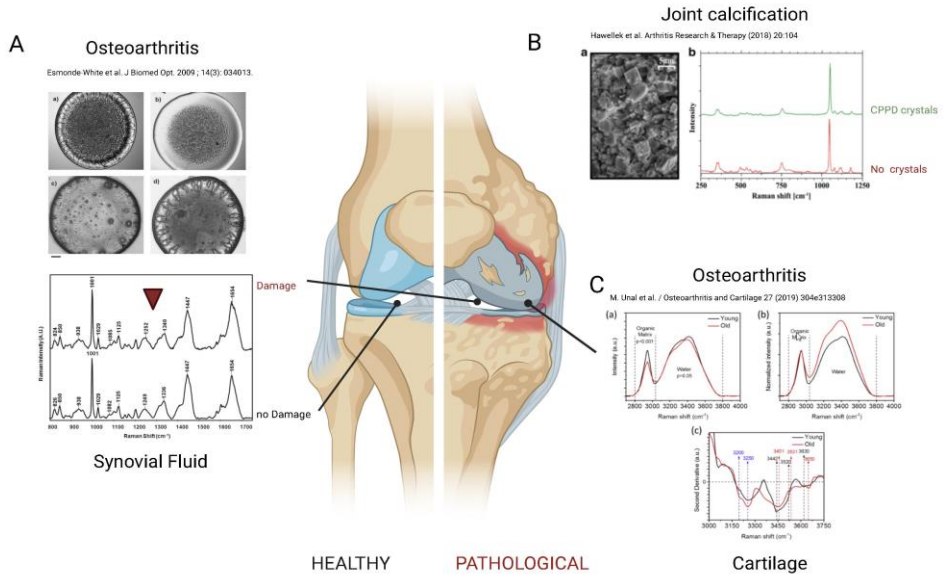

Figure 3: **Raman spectroscopy for the analysis of healthy and diseased joints**. (A) The biochemical composition of the synovial fluid from healthy subjects and osteoarthritic (OA) patients was analysed by Raman spectroscopy, showing the differences in protein secondary structures and content from OA patients. Figures are reproduced with permission from Esmonde-White *et al*. (doi: 10.1117/1.3130338).[84] (B) Differences in Raman Spectra can be found in diseased acetabular joint calcification. Figure reproduced with permission from Hawellek *et al*. (doi: 10.1186/s13075-018-1595-y).[85] (C) Variations in the water content in cartilage specimen showed altered spectra in young and old patients by Raman spectroscopy. Figure reproduced with permission from Unal *et al*. (doi:10.1016/j.joca.2018.10.003).[86] Figure created with Biorender.com

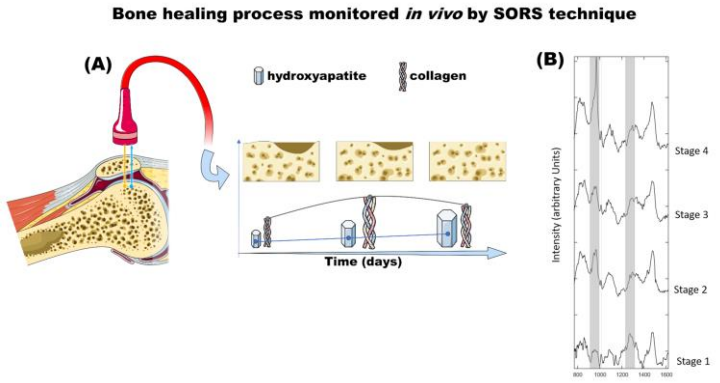

Figure 4: ***In vivo*** **monitoring of bone healing process by Spatially Offset Raman Spectroscopy (SORS).** (A) SORS can provide Raman signal arising from a defined depth, allowing to collect biochemical data from inner layers of living tissue. Intensity ratio of collagen (amide I, III) and hydroxyapatite (phosphate) Raman bands furnishes indication of bone healing status. (B) SORS spectra (after substraction of baseline) of collagen:HA phantoms inserted in rat skulls. Different stages of bone regeneration are characterized by specific collagen:HA ratio. Figure is reproduced with permission from Dooley *et al.* (doi: 0.1002/jbio.202000190).[111]

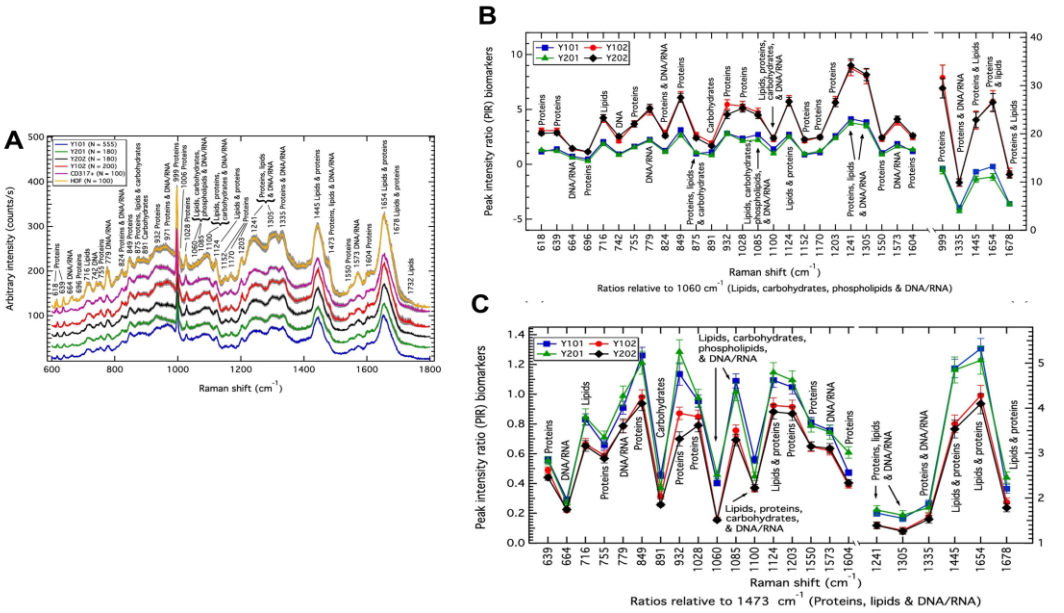

Figure 5: Mesenchymal stem cells characterisation (A) Average Raman spectra measured from 4 MSC cell lines originated from a common MSC pool. MSC positive control: CD317 + MSC. MSC negative control: HDF. PIR analysis of the spectra showed the discrepancy between differentiation-competent cells sub-population, and differentiation incompetent cells sub-population. Raman spectra showed discrepancies between the groups at the DNA/RNA, carbohydrates, lipids and proteins levels (1060 cm^{-1} band) (B), and the protein, lipids, DNA/RNA related band (1473 cm^{-1}) (C). Figures are reproduced with permission from Rocha *et al*. (doi:10.1038/s41598-021-81991-1)**.**[114]

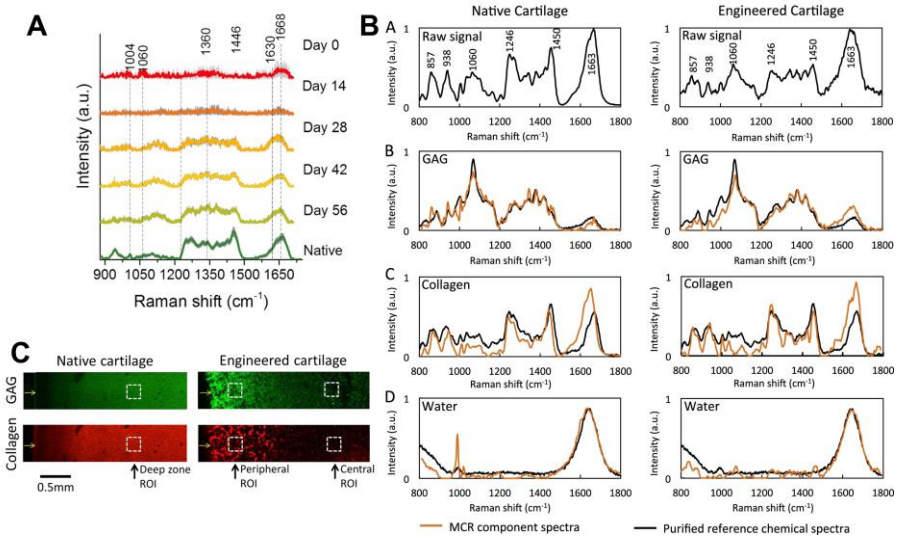

Figure 6: Quantitative and qualitative evaluation of tissue engineered constructs (A) Mean Raman spectra of TE cartilage construct cultures over time and native cartilage. Figure is reproduced with permission from Bergholt *et al*. (doi:10.1016/j.biomaterials.2017.06.015).[120] (B) Upper row: spectra of native cartilage and engineered cartilage. 2nd, 3rd, and 4th rows: protein specific spectra compared to correspondent purified proteins. (C) Raman semi-quantitative imaging of GAG and or collagen in native or tissue engineered cartilage. Figures in panels B and C are reproduced with permission from Albro *et al*. (doi:10.1038/s41536-018-0042-7).[121]

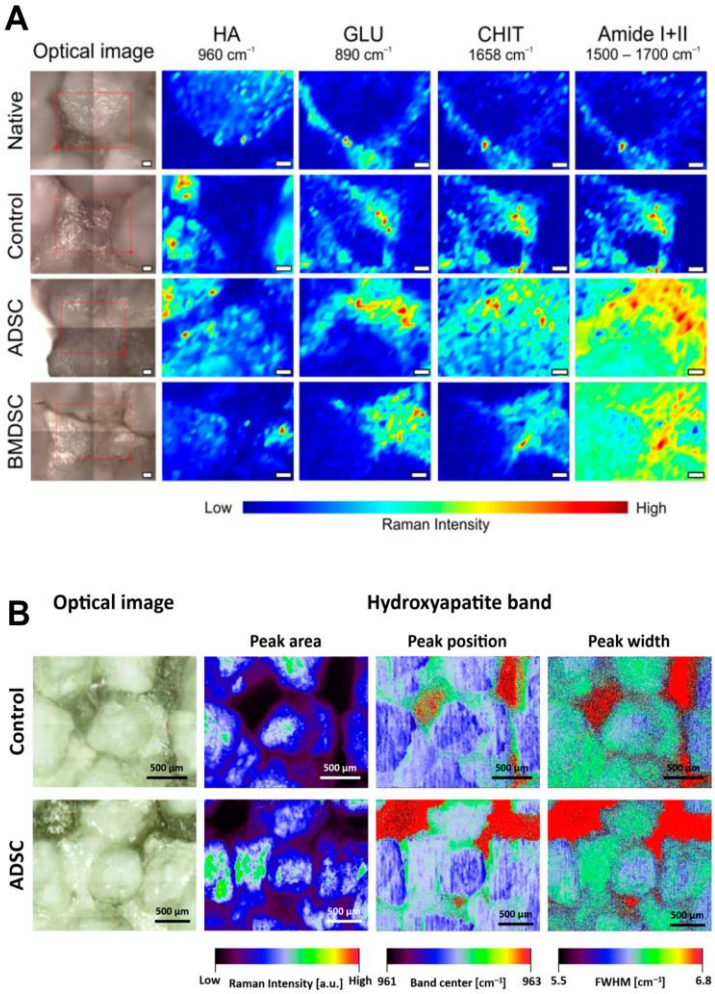

Figure 7: Raman assessment of cell-scaffolds interface. (A) Chemical mapping of scaffolds components in the presence or not of MSC. Amide I+II shows the distribution of the ECM at the MSC scaffold interface. (B) Raman imaging of HA phosphate deposition on scaffolds seeded or not with adipose derived MSC. Figures are reproduced with permission from Kalisz *et al*. (doi:10.3390/ijms22020485).[122]